*Journal of*
*Scanning Probe Microscopy*
Vol. 1, 3–20, 2006

# Atomic-Scale Spin-Polarized Scanning Tunneling Microscopy and Atomic Force Microscopy: A Review

Arthur R. Smith

*Nanoscale and Quantum Phenomena Institute, Department of Physics and Astronomy, Ohio University, Athens, Ohio 45701, USA*

REVIEW

Atomic-scale spin-polarized scanning tunneling microscopy is a powerful real-space technique for investigating the magnetic structure of surfaces. With its intrinsic lateral resolution capability, this technique can achieve atomic-scale resolved spin resolution of surfaces. Antiferromagnets, in particular, offer opportunities to test the spatial resolution of magnetism at ultimate length scales, where the magnetization reverses on the scale of one atomic spacing. In addition, the technique has been applied with very interesting results to the case of ferromagnetic surfaces. Reviewed here are the various contemporary experimental results, including a discussion of the theoretical basis for atomic-scale magnetic imaging. Theoretical calculations to simulate the magnetic STM images are also discussed, including those calculations which take into account the tip electronic structure.

**Keywords:** SP-STM, SP-AFM, Atomic-Scale, Spin-Polarized, Nanoscale Magnetism, Antiferromagnet.

## CONTENTS



## 1. INTRODUCTION

Within the last 25 years, great progress has been made in the field of nanometer science and technology. This is due to the invention of the scanning tunneling microscope (STM) by Binnig, Rohrer, and co-workers in 1981, which made possible the ability to actually "see" objects of nanometer size and even down to single atoms.[1] This unique ability to measure materials and devices at such exceedingly small length scales has resulted in astonishing details of materials previously only imagined. Simultaneous to the development of the field of STM and related scanning probe microscopies (SPM's), many great developments have also occurred in the electronics and magnetism fields. While the field of magnetism is arguably of equal importance as the field of electronics to society, it is amazing to note that within its first 25 years, STM was mainly used to study the *electronic* structure of surfaces. Only a tiny fraction of STM papers, most of them published within the last 6 years, have described the use of STM for measuring the *magnetic* properties of surfaces.[2–14] In the pages of these papers is found astonishing detail of the nanoscale magnetic structure of ferromagnetic (FM) and antiferromagnetic (aFM) surfaces.

In this review, it is attempted to gather a large subset (at least) of the important papers in the field of atomic-scale spin-polarized STM (SP-STM). Also discussed is one example of spin-polarized atomic force microscopy (SP-AFM), also referred to as exchange force microscopy. The treatment is primarily restricted to the presentation of those experimental and theoretical works dealing specifically with atomically resolved SP-STM or SP-STM in which the measured magnetic signal is directly correlated with atomic or fundamentally periodic structure, e.g., the periodicity of an antiferromagnet whose magnetic structure varies in sync with the orderly atomic structure of the material. First, the basic principle of SP-STM is described and a simple mathematical example given to motivate how the magnetic local density of states is involved in the spin-polarized imaging. Following this begins a

sequential discussion of the various experimental results which have been obtained using atomic-scale SP-STM and SP-AFM, including both antiferromagnets and ferromagnets (1 known case). Following this begins a section on theory, which includes two parts: first, a section dealing with the application of the spin-polarized Tersoff-Hamann formula with a discussion of the theory referred to as star coefficient theory and its applicability to various experimental cases and, second, a section dealing with the inclusion of the STM tip electronic structure in the calculations. Finally, the paper is briefly summarized with an outlook presented.

## 2. PRINCIPLE OF SPIN-POLARIZED SCANNING TUNNELING MICROSCOPY

Scanning tunneling microscopy, as is well known, is a powerful method for obtaining real space information about a crystal surface with resolution down to the atomic scale. In normal STM, a conducting sample surface is scanned using a conducting probe tip, and a non-spin-polarized tunneling current flows between the tip and sample. Probe tips commonly used for normal STM are fabricated from platinum–iridium and, more commonly, tungsten. For magnetic samples, however, magnetic contrast can be obtained using magnetic probe tips, and in this case a spin-polarized tunneling current flows between the tip and the sample. Suitable magnetic tip materials include nickel, iron, and $CrO_2$. More recently, magnetically coated W tips have proven highly successful.[3]

The basic working principle of spin-polarized STM is that, given that tip and sample magnetizations are vectors, the tunneling current will be larger when the vectors are parallel and smaller when they are antiparallel, with a cosine dependence for in-between orientations. The equation for tunneling current can be written most simply as:[2, 7]

$$I_t \sim \int [1 + P^t P^s \cos\theta]\, \mathrm{d}E \qquad (1)$$

where $P^t$ and $P^s$ are the spin polarizations of tip and sample, respectively. Variations in the tunneling current, dependent on the sample magnetization orientation, then allows the STM image to become a map of the spin polarization of the sample. This is more fully understood by considering that the tunneling current is actually composed of two components: a non-spin-polarized and a spin-polarized component. The spin-polarized component is normally zero in the case of nonmagnetic STM tips on nonmagnetic surfaces, but it becomes either negative or positive for a magnetic tip on a magnetic surface. In terms of the spin local density of states (LDOS), the tunneling current is written as:[15, 16]

$$I_t \sim \int g_V(E) \frac{1}{2} [n^t n^s + m^t m^s \cos\theta]\, \mathrm{d}E \qquad (2)$$

where $g_V(E) = f(E - E_F) - f(E - E_F - eV_S)$, $f$ being the Fermi function and $V_S$ being the applied sample bias; $n^t$ and $n^s$ are the total (spin majority + spin minority) LDOS of tip and sample, and $m^t$ and $m^s$ are the net magnetization (spin majority–spin minority) LDOS of tip and sample, respectively. Therefore, in SP-STM, what is really being measured is a quantity proportional to the convolution-integrated LDOS of sample and tip. It is important to notice that this integral is only over the window of energy defined by the Fermi level and the applied bias between sample and tip. Contrast in the constant current SP-STM image therefore depends on the spin polarization within this energy window between $E_F$ and $E_F + eV_S$; in $\mathrm{d}I/\mathrm{d}V$ imaging, magnetic contrast depends on the spin-polarization at $E_F + eV_S$.

An example of a convolution in the parallel case is depicted schematically in Figure 1(a) in which tip and sample are assumed to have LDOS functions which vary linearly with energy, as depicted, for both spin-↑ and spin-↓. The linear LDOS functions are chosen only for purposes of illustration; they will surely have more complicated functional forms in the case of a real sample and a real tip. We note that for sufficiently small voltages, it is often assumed that the LDOS of the tip is constant with energy over the relevant energy integration window. With that simpler assumption, qualitatively similar results to the example depicted in Figure 1 and discussed below would be obtained.

In the parallel case, for both sample and tip, the spin-↑ LDOS is majority. Note that both spin-↑ and spin-↓ LDOSs are positive values, although the spin-↓ LDOSs are plotted on the axis pointing down. In this example, the negative sample bias $V_s$ case is shown; note in this case the relevant sample states are filled while the relevant tip states

**Arthur R. Smith** completed his Ph.D. work at the University of Texas at Austin in 1995 in the area of cross-sectional UHV-STM of III–V semiconductor homo- and hetero-structures. After postdoctoral work at Carnegie Mellon University (1996 to 1998) focusing on wurtzite GaN surface reconstruction, he joined the faculty of the Physics and Astronomy Department at Ohio University. Since then, Smith's research has centered on MBE/STM of transition metal nitride materials, including gallium-, scandium-, chromium-, and manganese nitrides. In 2000, Smith was awarded the U.S. Presidential Early Career Award in Science and Engineering (PECASE). His first paper on atomic-scale spin-polarized STM of $Mn_3N_2$ was published in 2002. To date, he has 50 published papers. Smith was promoted to Associate Professor in 2003 and became director of Ohio University's Nanoscale and Quantum Phenomena Institute (NQPI) in 2005.

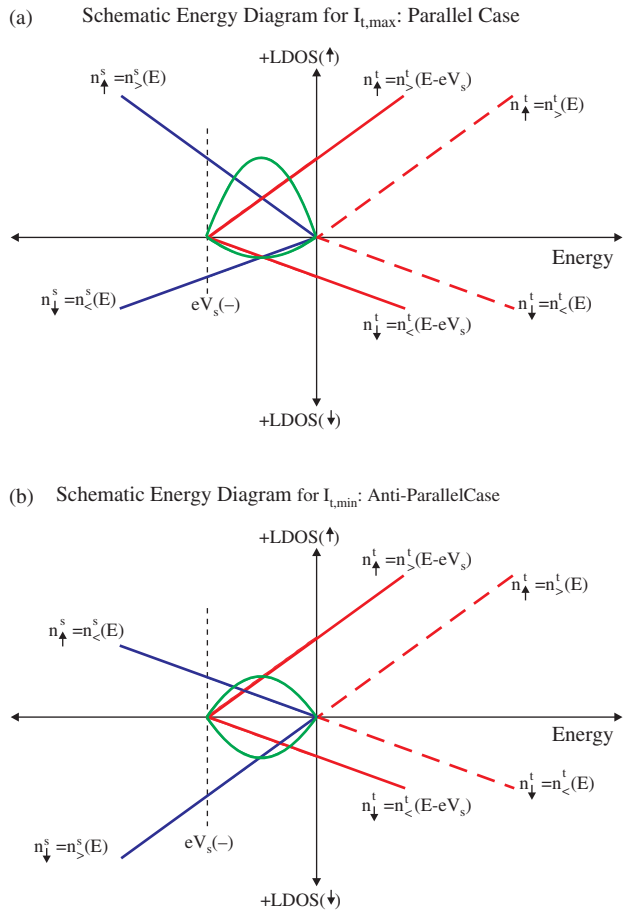


**Fig. 1.** Schematic energy diagrams of the spin-polarized overlap integrals in the simple case of a sample and tip whose LDOS vary linearly with energy. The sample bias is −1 V. The case in (a) corresponds to parallel tip and sample spins; the case in (b) corresponds to antiparallel tip and sample spins. Parabolas represent the products of the tip and sample LDOS over the energy range −1 to 0 eV.

are empty. For the parallel case, Figure 1(a) shows that the spin-↑ channel will compose the biggest part of the convolution integral, while the spin-↓ channel will compose the smallest part of the convolution integral. The parabolas shown in Figure 1 are the integrands of the convolution integrals. The sum of the areas (both positive areas) under the two parabolas is proportional to the total tunneling current. For purposes of the illustration let $n^t_>(E-eV_s)=4(E-eV_s)$/eV/atom, $n^t_<(E-eV_s)=2(E-eV_s)$/eV/atom, $n^s_>(\vec{R}_t,E)=-4E$/eV/atom, $n^s_<(\vec{R}_t,E)=-2E$/eV/atom. Note that all of these quantities are positive values over the energy window between $E_F$ and $(E_F+eV_s)$. Let $V_s=-1$ V. Then applying Eq. (2), the tunneling current $I_{t,\max}\sim(4\times4+2\times2)(1/6)=20/6$ (units of current), for the case of parallel tip and sample spin.

The convolution in the antiparallel case for the same negative sample bias $V_s$ is depicted schematically in Figure 1(b); here the sample spin-↑ LDOS is minority, while the sample spin-↓ LDOS is majority. In this case, the spin-↑ channel and spin-↓ channel will compose more similar integral values, as indicated by the areas under the parabolas shown in Figure 1(b). Using the LDOS functions given previously and applying Eq. (2), we get that the tunneling current $I_{t,\min}\sim(4\times2+4\times2)(1/6)=16/6$ (units of current), for the case of antiparallel tip and sample spin, which is less than $I_{t,\max}$.

This example illustrates that, in the case of a sample in which rows of atoms alternate in their majority and minority spin states (i.e., an antiferromagnet), the tunneling current is modulated as the tip scans across the rows in constant height (CH) mode, and the height of the tip will be modulated as the tip scans across the rows in the case of constant current (CC) mode.

## 3. ANTIFERROMAGNETIC SPIN STRUCTURE RESOLVED AT THE ATOMIC SCALE

A variety of antiferromagnets have been investigated using SP-STM, including first, single crystal chromium, and later aFM monolayers and thin films. In this section are discussed the published results to date in which SP-STM was used to resolve the antiferromagnet spin structure. The first paper which reported spin resolution on an antiferromagnet also happened to be the paper showing the first experimental SP-STM results. Lastly is discussed a recent report using spin-polarized atomic force microscopy to resolve the aFM spin structure.

### 3.1. Cr(001) Topological Antiferromagnetism

Wiesendanger et al. published the first SP-STM paper in 1990 on the topic of spin-polarized STM imaging of single crystal Cr(001).[2] Interestingly, the Cr(001) surface was predicted to be FM even though its bulk was well-known, from experiment and theory, to be aFM.[17,18] However, no previous experimental technique had been able to resolve any FM domain structure at the surface of Cr(001). Wiesendanger et al. imaged this surface using standard W STM tips, finding a step-terrace morphology with single monolayer steps of height ∼1.4 Å. Then, using $CrO_2$ tips, a similar morphology was found, except that the step height was found to alternate between two values, 1.2 Å and 1.6 Å.

This step height alternation was the first magnetic information ever observed using STM. It was interpreted as being due to the magnetic contribution from spin-polarized tunneling. The step height data were consistent with a surface morphology in which the FM spin direction of a given terrace reversed upon crossing single monolayer steps. Such topological antiferromagnetism had recently been proposed for Cr(001) by Blugel et al.[18] In this case, the STM tip would attain the same tunneling current at two characteristic distances from the surface, depending on the terrace. When the terrace magnetization was parallel to that of the tip, the CC tip–sample distance would increase slightly, whereas in the antiparallel case, the CC

REVIEW

tip–sample distance would decrease slightly. Then a step down from parallel to antiparallel would be a larger step, and a step down from antiparallel to parallel would be a smaller step.

Quantitatively, the change in tip–sample distance derived from the step height measurements was 0.10 Å, with an error half that amount, whereas the absolute tip–sample distance was determined to be ~5 Å. Although this represents only a 2% change in tip–sample spacing, a 0.10 Å change is quite easily measurable in a good STM.

Wiesendanger et al. also defined an "effective polarization" $P$ of the tunneling junction and gave an expression for it which depended on the tunneling constant $A \approx 1\ \mathrm{eV}^{-1/2}\ \mathrm{Å}^{-1}$, the surface work function $\phi$, and the measured step height difference from the average $\Delta s = 0.2$ Å. The authors measured $\phi$ to lie between 3 and 5 eV, concluding that the surface was clean during the measurements. Using the obtained numbers, the effective polarization was derived to be $(20 \pm 10)\%$.

While the results of Wiesendanger et al. clearly showed antiferromagnetism of a surface along the $z$-direction, the required lateral resolution needed was only that corresponding to the average terrace width of the surface and so did not make use of the intrinsic lateral resolution capability of STM. Another limitation of this result was that although the step heights could be easily measured, the magnetic and nonmagnetic (topographic) information contained within the whole SP-STM image was superimposed. The ability to decouple these two components would await future developments. Nonetheless, this first published work on SP-STM opened the gates to the important new field of SP-STM research and was the first SP-STM paper on antiferromagnetism.

### 3.2. Return to Cr(001): CC- and d*I*/d*V*-Mode Imaging

Ten years following the initial publication by Wiesendanger et al., Kleiber et al. published a new paper on the topic of Cr(001).[8] In this, they showed new results overcoming the limitations of the earlier work. In contrast to the use of $CrO_2$ tips, they used Fe-coated W tips as previously developed by Bode et al.[19] In the new work, two kinds of images were shown, including the CC-mode image of the same step-terrace structure seen in the earlier paper, but also the spectroscopic $\mathrm{d}I/\mathrm{d}V$-mode image. Whereas the CC-mode image contains both magnetic and nonmagnetic (topographic) contrast between adjacent terraces, the $\mathrm{d}I/\mathrm{d}V$-mode image contains only magnetic contrast between adjacent terraces. One then clearly sees the magnetization reversal at the step edges, making use of the lateral resolution of the STM, and that every other terrace has the same magnetization.

In addition to isolating the magnetic information using the $\mathrm{d}I/\mathrm{d}V$-mode imaging, Kleiber et al. also presented local tunneling spectroscopy results clearly identifying a surface state peak near the Fermi level $E_F$, whose intensity depended on the relative tip–sample magnetization orientation. Parallel orientation (in constant-separation mode) corresponded to greater peak intensity, whereas antiparallel orientation corresponded to smaller peak intensity. Kleiber et al. explain in detail how in the CC-mode the $\mathrm{d}I/\mathrm{d}V$ spectroscopic image shows the terrace with antiparallel tip–sample magnetization alignment brighter, while the terrace with parallel orientation is darker. In any case, the terrace-dependent magnetization is clearly resolved.

An additional accomplishment in this paper is the SP-STM imaging of the magnetization in the vicinity of screw dislocations. In this case, domain walls are found, and their width is measured to be 120 nm. Therefore, this is a very gradual change; atomically abrupt domain walls were found in a different system.

### 3.3. Atomically Abrupt Domain Walls: Fe on W(110)

One year after the publication by Kleiber et al.,[8] SP-STM was applied to the case of an ultrathin transition-metal film—in this case slightly greater than 1 monolayer of Fe on a vicinal W(110) substrate. The vicinal nature of the W(110) substrate led to the formation of narrow Fe nanostripes. Interestingly, although there is no hint of atomic resolution, the $\mathrm{d}I/\mathrm{d}V$ image clearly reveals the magnetic domains with, remarkably, domain walls having atomic-scale width of only ~6 Å. This and other results regarding domain walls near the atomic scale in FM layers are further discussed in another recent publication.[20]

### 3.4. Antiferromagnetic Mn Monolayer on W(110)

In 2000, Heinze et al. impressed the surface magnetism community, not to mention the greater nanoscale magnetism field, with their ground-breaking publication on the spin resolution of a Mn monolayer on W(110) substrate.[7] The nonmagnetic (morphological) structure of Mn grown at room temperature on W(110) was nicely demonstrated in a previous publication by Bode et al.[21] In that paper, the authors shows that Mn can be grown on W(110) pseudomorphically up to a local coverage of 3 ML. In their SP-STM experiment, such a pseudomorphic monolayer, grown at substrate temperature $T_{sub} \approx 400$ K, was prepared for study.

For the SP-STM study of Mn/W(110), Heinze et al. chose to focus on the first Mn monolayer. First principles theory had suggested that this monolayer should have a $c(2 \times 2)$ aFM ground state in which, at some low-enough temperature, the magnetic moments of adjacent nearest-neighbor atoms would point in opposite directions.

They imaged this Mn monolayer with three kinds of tips:
(1) plain W tips,
(2) Fe-coated W tips, and
(3) Gd-coated W tips.

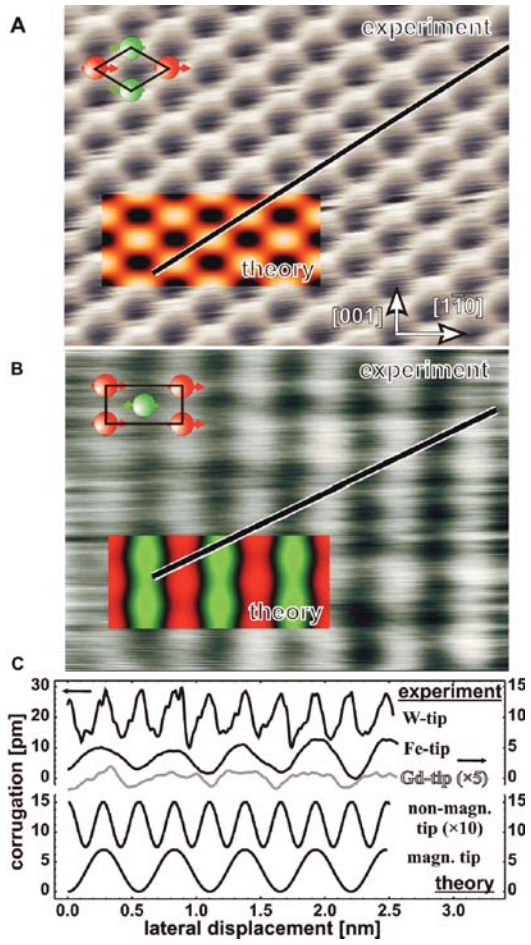


**Fig. 2.** Comparison of experimental and theoretical STM images of a Mn ML on W(110) with (A) a nonmagnetic W tip and (B) a magnetic Fe tip. (C) Experimental and theoretical line sections for the images in (A) and (B). The unit cell of the calculated magnetic ground-state configuration is shown in (A) and (B) for comparison. Tunneling parameters for both images are $I_{tun} = 40$ nA and $U = -3$ mV. The image size is 2.7 nm × 2.2 nm. Reprinted with permission from [7], S. Heinze et al., *Science* 288, 1805 **(2000)**. © 2000, AAAS.

Using the plain W tips, the atomic resolution image of each Mn atom site in two dimensions was obtained. This is shown in Figure 2(a), in which a 27 Å × 22 Å area is resolved. Theory computations were compared with the image, as shown in the inset of Figure 2(a). As can be seen, the agreement between theory and experiment was shown to be quite good. Next, they applied the Fe-coated W tip to image a Mn monolayer. Bode et al. had previously shown that these tips possessed magnetization axes in the plane of the sample.[19] This was considered important since theory suggested that the easy axis should be *in-plane*, and only if the tip and sample magnetization axes have a common vector component is it possible to obtain magnetic contrast. Given such a tip, it might be possible that atomic-resolved images would reveal the spin structure of each atom, a positive or negative signal superimposed on the normal, atomic-resolution image. What they found was completely different.

The image resulting from the use of the Fe-coated W tip is shown in Figure 2(b). What was completely surprising to the researchers was that rather than each atomic site having superimposed upon it an enhancement or a depression depending on the spin alignment of sample and tip, the magnetic tip resulted in an image consisting just of stripes running along the [001] direction. This was the case for either the Fe-coated or the Gd-coated W tips. These stripes had a periodicity equal to two atomic-row spacings along the $[1\bar{1}0]$ direction. All evidence of a nonmagnetic signal, as shown with the nonmagnetic W tip in Figure 2(a), had vanished.

It was then discovered that the stripes were exactly what was predicted by first-principles theory, as seen by the theory simulation shown in the inset of Figure 2(b). This is not unreasonable, considering that every other [001] row consists of atoms with the same spin direction. The magnetic STM imaging therefore resolved the spin of the surface in rows, but in addition, along the [001] row direction, a slight modulation of the row height, predicted by the theory simulation, was apparent.

Still, what was particularly surprising was that the spin-polarized image was entirely magnetic; there was no nonmagnetic component. This eliminated the need for any decoupling of magnetic and nonmagnetic information. The application of a magnetic tip resulted in a magnetic image, while the application of a nonmagnetic tip resulted in a nonmagnetic image. A simple explanation for this contrast behavior can be made in terms of surface periodicities; it turns out that, in this case, the magnetic tip sees a much bigger response to the magnetic period in comparison with the twice smaller, atomic period, whereas the nonmagnetic tip only responds to the smaller atomic period. This is explained in more detail in Section V.

The paper by Heinze et al. was the first convincing demonstration of antiferromagnetism resolved at the atomic scale in the *in-plane* direction. Nonetheless, new and different results waited to be demonstrated in different systems, yielding new insights into the ultimate limits of magnetic imaging.

### 3.5. Antiferromagnetic $Mn_3N_2$(010) Thin Film on MgO(001)

#### *3.5.1. Epitaxial Growth of $Mn_3N_2$*

Two years after the publication of Heinze et al.'s Mn ML on W(110) result, observations of spin resolution of an aFM thin film of $Mn_3N_2$(010) were published by Yang et al.[14] Results from this study provided new compelling evidence for atomic-scale spin-resolved STM, while at the same time presenting additional aspects not seen in the Heinze et al. results.

The initial motivation to study manganese nitride sprang from an interest in the widely varying and interesting magnetic properties of the different phases of this material.

Up to ca. 2000, manganese nitride had been studied in bulk or thick film form by a number of authors, and much was already known about its phases, stoichiometries, crystal structures, lattice constants, and magnetic properties, which to this day show great promise for future technological applications.[22–31] However, regarding the epitaxial growth of thin films and layers of this material, relatively little if anything was known. And technological applications involving their magnetic and electronic properties would require a sound knowledge of their epitaxial growth.

An additional motivation for studying manganese nitride stemmed from the growing interest in magnetic-doped nitride semiconductors, which began from a single theory paper.[32] In that one paper, Dietl et al. had predicted that Mn-doped GaN (and also ZnO) may be a dilute FM semiconductor at room temperature if the doping concentration, carrier type, and carrier density satisfied certain stated conditions. From this perspective, if a ternary compound based on manganese nitride and gallium nitride was to become important technologically for the new field referred to as *spintronics*, then it should also be important to fully explore the epitaxial growth of the two binary compounds; moreover, epitaxial growth of GaN was already far advanced.

Smith et al. thus began to study manganese nitride in ca. 2000, with the goal to grow thin films using molecular beam epitaxy and study them using STM. The first findings of this study were published by Yang et al. in 2001.[33] Under certain Mn-rich growth conditions, an (010)-oriented, aFM $Mn_3N_2$ thin film grew epitaxially on top of the oxide MgO(001), which was used as substrate. By varying the manganese flux, it was possible to reorient this film to the (001) orientation during growth. Furthermore, by varying both the manganese flux and the substrate temperature, it was possible to control both the phase and orientation.[34]

Yang et al. showed that by using a W tip, the STM image of $Mn_3N_2(010)$ shows a rowlike structure within each of two 90°-rotated domains. That rowlike structure was shown to correspond perfectly with the (010) termination of the bulk $Mn_3N_2$ structure. The bulk structure of $Mn_3N_2$ was known from the work of Jacobs et al., and it consists of a face-centered tetragonal lattice with a 2 atom (Mn and N) basis set; this is the rock-salt type structure.[27] For the (010) surface, the spacing of the rows corresponded to the spacing between planes of nitrogen vacancies in the bulk model; these occur every third atomic layer along the (001) direction. The [001] direction is therefore parallel to the (010) film surface and perpendicular to the [100]-aligned rows seen in the STM image.

Zoom-in images of the $Mn_3N_2(010)$ surface using ultrasharp STM tips revealed each Mn atom of the surface. Those along the center of the row appeared bright, while for each bright atom, there were two darker atoms off-center of the row. The detailed study of the tip-sample bias dependence of the contrast in these atomic-scale resolved STM images was shown later by Yang et al. and compared with theory predictions based on bulk first-principles LDOS calculations by Lambrecht.[35] Good agreement was found between experiment and theory. Lambrecht et al. also published a theory paper showing that for both MnN and $Mn_3N_2$, the Mn-atom LDOS is dominant over N-atom LDOS near the Fermi level;[36] the STM images therefore show only Mn atoms.

### *3.5.2. Spin Resolution of $Mn_3N_2(010)$ using SP-STM*

In their work (2002), Yang et al. used Mn-coated and Fe-coated W tips to image the $Mn_3N_2(010)$ surface.[14] According to the simple bulk picture, every adjacent [100] row of atoms at the surface should have opposite spin direction. In typical STM images, the row structure has periodicity of 3 times the simple atomic-row spacing. Therefore, even this 3-by superstructure should be aFM as understood by the following sequence: $\ldots \Uparrow \downarrow \uparrow \Downarrow \uparrow \downarrow \Uparrow \downarrow \uparrow \Downarrow \uparrow \downarrow \Uparrow \downarrow \uparrow \Downarrow \uparrow \downarrow \ldots$ Here, the double arrows denote those spins with $3\times$ spacing and which form an aFM sequence as well as the primitive spin sequence with $1\times$ spacing. In fact, we may consider that the double arrows represent the spins of the Mn atoms in layers without N (with N vacancies), called Mn1 atoms, and that the single arrows represent the spins of the Mn atoms in layers with N, called Mn2 atoms.

The SP-STM image produced using a Mn-coated W tip, at room temperature, is shown in Figure 3(a). There, two 90° rotated domains intersect along a domain boundary, which is both a crystallographic as well as a magnetic domain boundary. Seen in either domain D1 or domain D2 is the row structure with $3\times$ period in comparison to the primitive atomic spacing. Clearly distinguishable is that adjacent rows have different brightness and that the brightness alternates from row to row. This brightness alternation is clearly seen in the height profile shown in Figure 3(b), which shows a modulation having a period of 2 rows. Line profiles from both domains D1 and D2 show the modulation, and a simple spin model of the boundary region is depicted in Figure 3(c). Clearly, the height modulation of the rows corresponds to the aFM double-arrow sequence previously given and the observation of a modulation means that the SP-STM data contain two components, one magnetic and one nonmagnetic.

Seeing also that the magnitude of the height modulation shown in Figure 3(b) is different on the two sides of the boundary, in the inset of the model of Figure 3(c), a probable vector relationship is given for the tip spin and spins from either side of the domain boundary. Yang et al. noted the cosine relationship for the amplitude modulation and derived the tip-sample spin angle in their experiment to be $\sim 27°$.

Yang et al. went on to show a method to separate the two components out from the height profile. This method

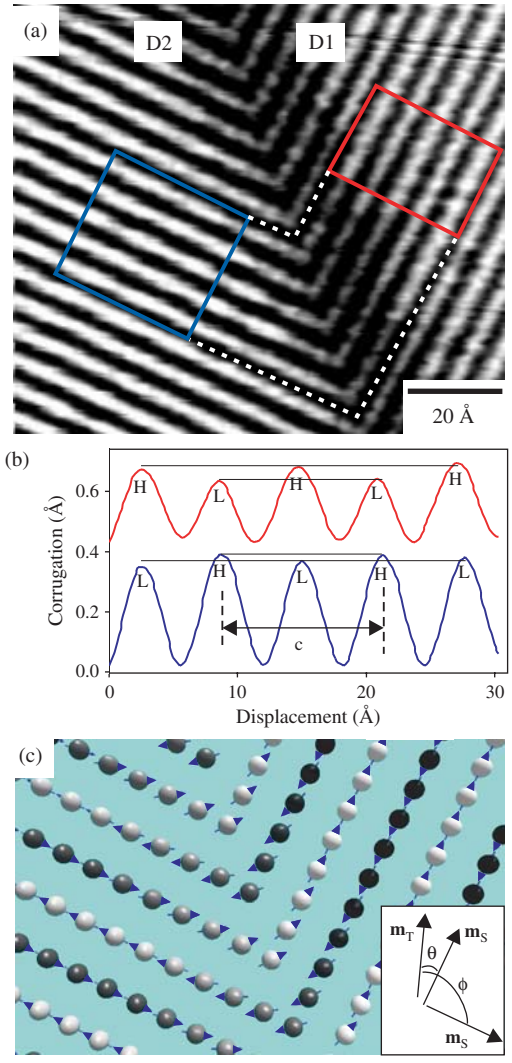


**Fig. 3.** (a) SP-STM image acquired using a Mn-coated W tip at $V_s = -0.6$ V and $I_t = 0.8$ nA. (b) Two area-averaged line profiles (red and blue) corresponding to the regions inside the red and blue rectangles in (a). (c) Simulated SP-STM map: contrast: white ↔ black ⇒ $\theta$: $0 \leftrightarrow \pi$. The inset shows the moments of tip ($\mathbf{m}_T$) and the sample ($\mathbf{m}_S$) for the two different domains and the angles between them. Each ball represents a magnetic atom. Reprinted with permission from [14], H. Q. Yang et al., *Phys. Rev. Lett.* 89, 226 101 **(2002)**. © 2002, American Physical Society.

was explained mathematically in the paper and involved essentially subtracting the $\pi$-shifted line profile from the nonshifted line profile to obtain the magnetic part and adding these two to obtain the nonmagnetic part. Doing so revealed a sinusoid-like nonmagnetic component but a non-sinusoid-like (in fact, trapezoid-like) magnetic component at the bias voltage of $V_S = -0.6$ V. Consistent results were also obtained with an Fe-coated W tip.

Yang et al. also went on to model the two components separately using LDOS values obtained from bulk first principles inserted into an atom-superposition model. Nice agreement between theory and experiment was shown. Simulations based on the full Tersoff-Hamman model with surface LDOS calculated from first principles (by A. Dick and J. Neugebauer) were presented in a later paper by Smith et al.[15] That paper highlighted the shortcomings of the atom superposition method (i.e., comparisons of STM data to atom superposition simulations can be fortuitous; for reasons, see Ref. [15]) and underscored the importance of directional orbital lobes in SP-STM imaging and simulations.

### *3.5.3. Bias Dependence of Spin Resolution of $Mn_3N_2(010)$*

Bias dependence in atomic resolution images of surfaces is closely related to the spectroscopic information, and by studying the bias dependence, additional information about the surface is often obtained. In the case of $Mn_3N_2(010)$, such data were recently reported (2004) by Yang et al. for the case of nonmagnetic probe tips. What was clear from the bias-dependent CC height profiles was that the overall magnitude of the height profile was maximized near $V_S = +0.2$ V and that it gets smaller with increasing positive or negative voltage. This behavior was shown to be in good agreement with the amplitude values calculated based on atom superposition simulations using LDOS values calculated from bulk first principles.

In the case of atomic-resolved magnetic STM images of the same surface, Smith et al. have investigated the magnetic amplitude dependence on the bias voltage, as recently reported (2005).[37] Shown in Figure 4(a) is the sequence of spin-polarized STM images, acquired from the same exact surface location, of $Mn_3N_2$ (010) between $V_S = -0.6$ V and $V_S = +0.6$ V, in 0.2 V increments (not including 0). These images were acquired using an Fe-coated W tip. What is prominently seen in these images is the row structure, in which the observed atomic rows are centered at the Mn1 atoms.

Below each image in Figure 4(a) is displayed the total CC height profile. Clearly, the data contain spin-resolved information, according to the evident modulation of the height profiles. Upward pointing red arrows, located at positively enhanced peaks, correspond to spin-↑; in-between, negatively enhanced peaks correspond to spin-↓.

To understand the experimental data more clearly, in Figure 4(b) is a diagram showing a schematic spin-polarized STM line profile together with the atomic model of the $Mn_3N_2(010)$ surface, including magnetic moment vectors and labels of Mn1, Mn2, and N atoms. From this diagram, it is seen that the rows of the STM images are centered on the Mn1 atoms and that the height modulation of the rows corresponds to the alternation in magnetic vector direction of the Mn1 atoms.

Of particular interest in Figure 4(a) is the observation of a magnetic contrast inversion point at $V_S \simeq +0.4$ V. At bias voltages less than +0.4 V, there are two high peaks

REVIEW

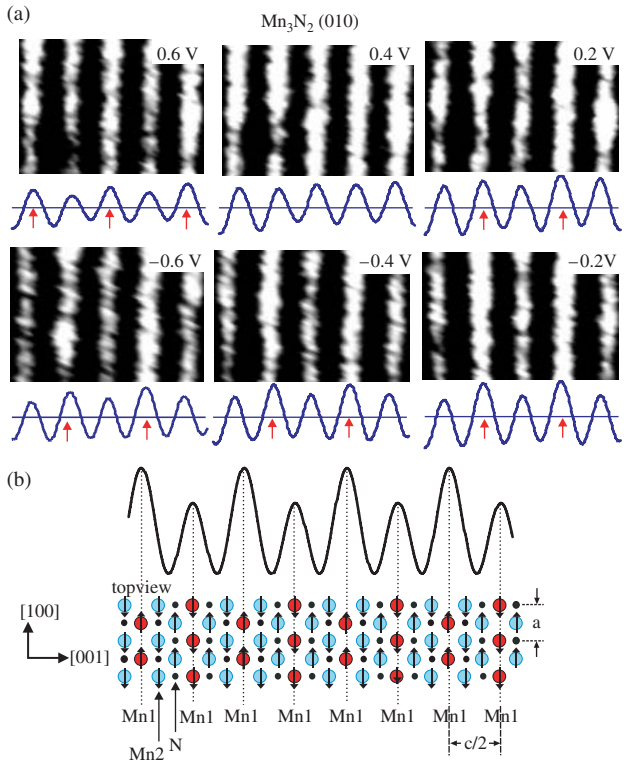


**Fig. 4.** (a) A series of SP-STM images of $Mn_3N_2$(010) acquired using an Fe-coated W tip taken at the exact same surface location. The sample bias is indicated in each part, and tunnel current $I_t = 0.3$ nA. Height profiles below each image are averages over the vertical direction of the corresponding image. (b) Diagram of spin-polarized STM line profile with atomic model of the $Mn_3N_2$(010) surface, including magnetic moment vectors. Reprinted with permission from [37], A. R. Smith et al., *Recent Adv. Atomic-Scale Spin-Polarized Scanning Tunneling Microsc., Microsc. Res. Technique* 66, 72 **(2005)**. © 2005, Wiley-Liss, Inc.

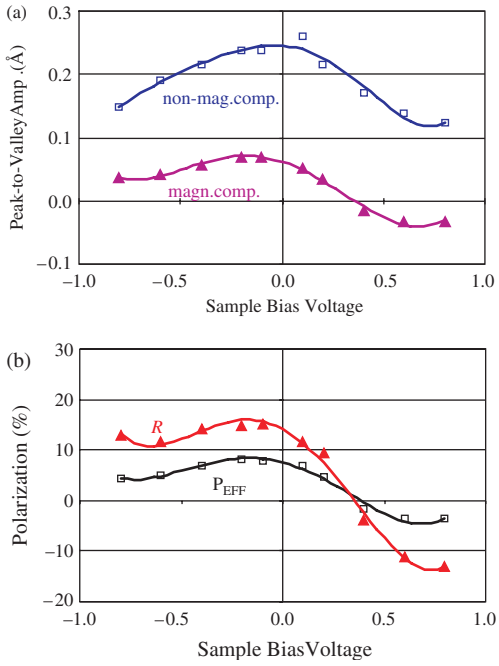


**Fig. 5.** Peak-to-valley amplitudes of magnetic (purple) and nonmagnetic (blue) components of the height profile as a function of sample bias. (b) The deduced junction polarization $P_{EFF}$ from STM data (black) and the ratio $R$ of one-half the magnetic peak-to-valley amplitude to non magnetic peak-to-valley amplitude versus sample bias from STM data (red). Reprinted with permission from [37], A. R. Smith et al., *Recent Adv. Atomic-Scale Spin-Polarized Scanning Tunneling Micros., Microsc. Res. Technique* 66, 72 **(2005)**. © 2005, Wiley-Liss, Inc.

and three low peaks in the series, whereas at bias voltage greater than +0.4 V (i.e., 0.6 V), there are three high peaks and two low peaks. This information is summarized in Figure 5(a), which shows the experimental nonmagnetic and magnetic amplitudes over an even larger number of points. These values were obtained after separation of the magnetic and nonmagnetic information contained within the data of Figure 4(a). In Figure 5(b) are shown two additional derived quantities: $R$ = one-half the magnetic to nonmagnetic amplitude ratio, and $P_{\text{eff}}$, the effective junction polarization, which was defined by Wiesendanger et al.[2]

The nonmagnetic bias-dependent amplitude shows very good agreement with our previously published data using nonmagnetic STM tips.[35] Here we want to focus on the magnetic amplitude. The important issue is whether this bias dependence is a function of the sample electronic structure or that of the tip. As it is widely accepted, ever since the original work of Tersoff and Hamann,[38] that what the STM images in normal STM is the LDOS of the sample (not the tip) near the Fermi level, it is important to assess if this is also the case in magnetic STM. This can only be determined by performing careful first principles surface calculations and then inserting the results into a spin-polarized form of the Tersoff-Hamann formula. A new paper combining experiment and theory, addressing this exact issue, is being finalized in parallel with this review.[39]

### 3.6. Antiferromagnetic Fe Monolayer on W(001)

The interest in the magnetic properties of iron has existed surely since man's earliest encounter with this material. Mainly, iron has proven to be one of the best ferromagnets ever known, in its bcc bulk structure. However, there has been much study to try to stabilize Fe in other magnetic states via different crystal structures or using novel strategies. One strategy is to take advantage of low-dimensionality, such as a single ML of Fe (2-D) on a particular substrate. One such system, namely, a ML of Fe on W(001), was examined in the early 1990s, and clear experimental evidence was obtained, using spin-resolved photoemission[40] and Kerr effect measurements,[41] showing a lack of remanence and arguing against a FM ground state. Density functional theory lent support to the possible existence of a lowest energy aFM Fe ML state.[42]

In very recent work (2005), Kubetzka et al. demonstrated convincingly that a single ML of Fe on W(001) has

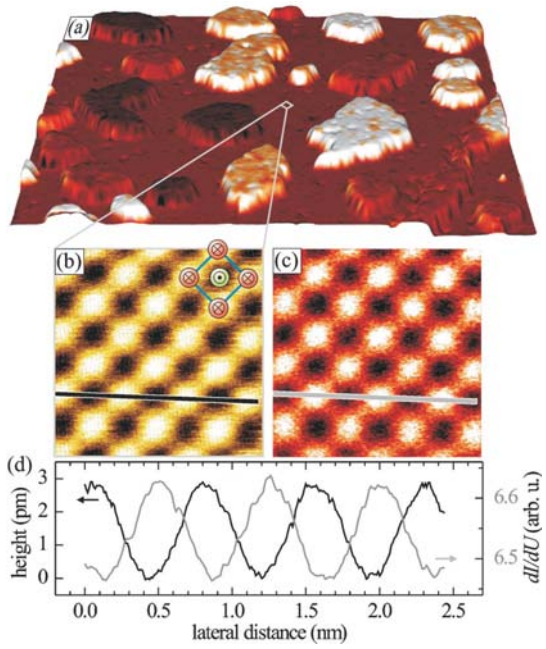


**Fig. 6.** (a) 3D composite of topography (height) and $d\mathrm{I}/d\mathrm{U}$ signal (color) of a $100 \times 100$ nm$^2$ surface area of 1.3 ML Fe/W(001) ($I = 2$ nA, $U = 500$ mV). In zero field a four-stage magnetic contrast is observed on the second layer islands. In an external field of $B = +2.5$ T the ML shows a $c(2 \times 2)$ superstructure in (b) the constant current image as well as in (c) the corresponding $d\mathrm{I}/d\mathrm{U}$ map ($2.5 \times 2.5$ nm$^2$, $I = 3$ nA, $U = -100$ mV). (d) Line sections along the [100] direction. Reprinted with permission from [43], A. Kubetzka et al., *Phys. Rev. Lett.* 94, 087 204 (**2005**). © 2005, American Physical Society.

indeed an aFM ground state, using atomic-scale SP-STM.[43] In this paper, they place their work well into the experimental and theoretical context but utilize the unique atomic-scale magnetic resolution capability of SP-STM to prove that the magnetic ground state is aFM $c(2 \times 2)$. They also show that the magnetization is *out-of-plane*.

Shown in Figure 6(a) is the large-scale image of the surface containing 1.3 ML Fe on W(001). Islands of the second layer are seen clearly within the area; their different color can be interpreted in terms of the FM vector orientation of these second-layer islands. For a more general study of the morphological and magnetic structure of the Fe/W(001) system in the pseudomorphic regime, including islands up to the 4th ML, see the recent paper by Von Bergmann et al.[44] The focus of the atomic-scale SP-STM study is on the areas in between the second ML islands, which are the areas having just 1 pseudomorphic ML of Fe on W(001). Zoom-in images of a tiny area of the 1 ML Fe region are shown in Figure 6(b) and (c). Figure 6(b) shows just the normal constant current STM image of the region, while Figure 6(c) is the $d\mathrm{I}/d\mathrm{V}$ spectroscopic image of the same region.

Clearly, both CC and $d\mathrm{I}/d\mathrm{V}$ images show an atomic-scale checkerboard pattern, whose interpretation is well explained by Kubetzka et al. As discussed previously, for the case of a Mn ML on W(110) published by Heinze et al.,[7] the first remarkable point is that, in these images also, only magnetic contrast is observed; the normal atomic resolution image observed using a nonmagnetic W tip would show twice as many bright spots. It turns out that the bright spots of Figure 6(b), however, correspond only to the atoms of spin down, whereas the dark "holes" correspond to the atoms of spin "up" [see Fig. 6(b), model overlay]. As also clearly seen in Figure 6(b) and (c), the CC and $d\mathrm{I}/d\mathrm{V}$ images are 180° out of phase, as shown also in the line profile of Figure 6(d).

To achieve this remarkable result, Kubetzka et al. used an Fe-coated W tip, which normally shows *in-plane* magnetic contrast, in the absence of an applied magnetic field. However, the images shown in Figure 6 were not obtained in zero field but instead were obtained using the unique capability of their STM, which allows application of large perpendicular magnetic fields of magnitude 2.5 T. They explain that such a field is sufficient to rotate the magnetization of the Fe-coated tip into the *out-of-plane* direction. After doing this, the aFM contrast of the Fe ML is obtained. Then, knowing that, in SP-STM, magnetic contrast is only seen for the case where sample and tip have a common vector component, it can be concluded that the sample magnetization is also *out-of-plane*. It is also understood here that the applied magnetic field, although rotating the FM tip magnetization vector, should leave the aFM layer magnetization unaffected.

In their paper, Kubetzka et al. also present side-by-side images of a small surface region obtained in opposite magnetic fields of +2.5 T and −2.5 T. Such fields will polarize the FM tip coating oppositely, and both images show clear magnetic contrast, but 180° out of phase. Then by subtracting the two images, the purely magnetic image is obtained showing the clear $c(2 \times 2)$ aFM contrast, and by adding the two images, the purely nonmagnetic image is obtained. Mathematically, this approach is equivalent to the difference/sum method used by Yang et al. to separate out the magnetic and nonmagnetic components from their SP-STM line profiles of $Mn_3N_2(010)$, as previously discussed. In Kubetzka et al.'s case, however, while the magnetic image shows clearly the aFM structure, the nonmagnetic image does not show any underlying atomic features.

A nice outlook of the paper by Kubetzka et al. is the possibility to tune the substrate/overlayer interaction by varying the substrate lattice constant, for example, through the use of alloys, with the possibility of obtaining a variety of new magnetic overlayer structures.

### 3.7. Antiferromagnetic NiO(001) Surface: Spin-Polarized AFM

Although SP-STM is limited to conducting samples, other investigators have recently been attempting to make use of the magnetic exchange force interaction as another means to detect spin direction at a sample surface. Atomic force microscopy (AFM) is well-known as a method for

imaging insulating as well as conducting samples. The use of noncontact AFM (NC-AFM) to study surfaces has proven to be successful for obtaining resolution down to atomic scale. If then a magnetic exchange interaction would exist between a magnetic probe tip and a magnetic surface, then a component of the total force interaction could be attributed to be of magnetic origin; therefore, the NC-AFM image could potentially contain spin-dependent information.

A key question in recent years has been concerned with what the size of the magnetic exchange force which could be expected is and whether then it would be large enough to be detected. A number of theoretical calculations were published on this topic.[45–48] The conclusion of these works suggests that the exchange interaction between a FM tip and a FM sample would indeed be sufficiently large for detection using conventional NC-AFM available instrumentation.

The use of FM atomic force microscopy tips on FM sample surfaces is chiefly thought of as the method of magnetic force microscopy (MFM). The technique of MFM, however, has lateral spatial resolution limited to approximately several tens of nanometers, due to the fact that the relevant interaction is the long-range dipole interaction involving the stray field of the sample and tip. The long-range interaction has nothing to do with the exchange force as a means of spin measurement. However, to overcome the dominating effect of the long-range dipole interaction, and to obtain sensitivity to the much weaker short-range exchange interaction, an ideal approach is to utilize either an aFM tip, an aFM sample, or both.

In two recent (2004) papers, Hosoi and co-workers have shown promising results using just this kind of approach.[49, 50] In their reported experiments, they have applied ultrahigh vacuum NC-AFM operating at room temperature, with three different types of probe tips:

(1) Fe-coated Si tips,
(2) Ni-coated Si tips, and
(3) nonmagnetic Si tips.

For their sample, they selected the well-known room-temperature aFM insulator NiO and as the surface of study NiO(001). The crystallographic model of NiO with spin alignment, as shown by the authors, is reproduced in Figure 7(a). A key point is that along the [110] direction, spins are antiferromagnetically aligned, while along the $[1\bar{1}0]$ direction, spins are ferromagnetically aligned; this point is utilized in the analysis of Hosoi et al.

The sample and tip were each outgased under vacuum, using a mild heating step. The Si cantelever tips were coated by Fe (or Ni) to a coating thickness of 30 nm. The NiO(001) surface was prepared by cleaving the NiO bar in UHV.

NC-AFM images using the three different types of tips were obtained, each showing atomic resolution. In their papers, the authors present the image obtained using the

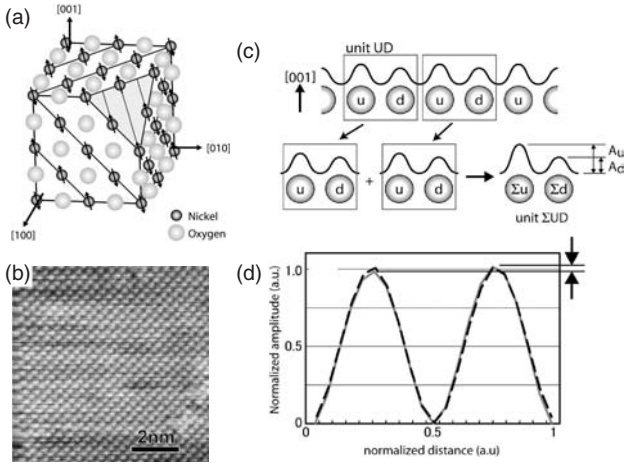


**Fig. 7.** (a) the crystallographic structure of NiO single crystal with spin alignment. The spins at Ni sites on {111} planes are ferromagnetically aligned, and the direction of spin in the adjacent planes is antiparallel. (b) Atomically resolved image obtained with an Fe-coated tip (8.1 nm × 8.1 nm. (c) Conceptual scheme of atomic corrugation analysis. The cross-section is divided into the unit cell (UD) composed of adjacent atoms *u* and *d*. Their corrugation amplitudes are added, and the maximum values at each atom site are compared by means of topographical asymmetry. (d) The added corrugation amplitude taken from (b) in the [110] (full gray curve) and the $[1\bar{1}0]$ (dashed black curve) direction. Reprinted with permission from [49], H. Hosoi et al., Investigations on the topographical asymmetry of non-contact atomic force microscopy images of NiO(001) surface observed with a ferromagnetic tip. *Nanotechnology* 15, 505 (**2004**). © 2004, IOP Publishing Ltd.

Fe-coated Si tip. This image, reproduced in Figure 7(b), shows a square array of atomic protrusions, whose vertical corrugations are ∼0.3 Å; no obvious height differences can be seen in the image between the different protrusions. The authors give arguments to decide whether the protrusions observed correspond to the Ni or to the O atoms. A number of prior studies would suggest that it is the O atom which is the protrusion in images acquired using metallic probe tips.[51–54]

It is therefore concluded in the work of Hosoi and co-workers that the NC-AFM image of NiO(001) obtained using the metallic coated (Fe or Ni) probe tips shows protrusions which correspond to the O atoms. They go on then to analyze in detail the line profile corrugations, looking for indication of spin contrast. While none appears in the image upon visual inspection, a method is presented to enhance the signal-to-noise ratio by superimposing groups of line scan pieces representing identical magnetic structures. This method is shown schematically by Hosoi et al., as reproduced in Figure 7(c). The results of the data processing for the data shown in Figure 7(b) are reproduced in Figure 7(d), where a slight difference in corrugation maxima between adjacent atomic sites along [110] can be detected.

To lend statistical significance to the relatively small effects, Hosoi and co-workers define a quantity called topographical asymmetry $A = (A_u - A_d)/(A_u + A_d)$, with

$A_u$ and $A_d$ being the maxima of the superimposed corrugations at the adjacent *u* and *d* atom sites, respectively. This quantity is computed for different azimuthal directions of the surface.

As discussed by Hosoi and co-authors, by comparing *A* along [110] versus *A* along [1$\bar{1}$0], a difference can be seen, with *A* almost 1.5% for [110] versus ~0.4% for [1$\bar{1}$0]. The authors then proceed to tabulate results from the various magnetic coated and nonmagnetic coated tips in the same way, and based on those numbers, they argue that the magnetic-coated tips show statistically significant magnetic effects in comparison to the nonmagnetic Si tips. However, they do note some inconsistencies among the different tips, for which they present some possible explanations.

Assuming that these very small measured asymmetries are reliable, then it is important to understand their origin. One of the key points raised in the works by Hosoi and co-workers is that although the protrusions correspond to O atoms, the magnetic moments in NiO are carried by the Ni atoms; how then, can one understand the observed corrugation asymmetries? This question is addressed in a recent first-principles theoretical study by Momida and Oguchi.[55] They study exactly the NiO system realized by Hosoi and co-workers. One of the key points in their work is that the surface O takes on a moment due to surface symmetry breaking, although it is small (~0.07 $\mu_B$). This is due to hybridization between the surface O atom p states and the second-layer Ni atom d states. Moreover, the first-layer O atom moment is parallel to the second-layer Ni atom moment, rendering the same aFM surface symmetry for O atom sublattice as for Ni atom sublattice.

While the approach of NC-AFM to image magnetic structure by means of the exchange force interaction will require more study to fully understand, the work of Hosoi et al. represents the ultimate in what has been achieved to date in atomic-scale SP-AFM imaging. Although this method offers applicability to insulating materials such as NiO, the sensitivity of the method appears to be a significant potential limitation.

## 4. ATOMIC-RESOLVED SPIN-STRUCTURE IN FERROMAGNETS

Although antiferromagnets are ideal subjects for observing atomic-scale spin variations, or alternations, the power of the SP-STM is its ability to detect either changes in the local spin direction, or changes in the local spin-polarization density. In the case of a ferromagnet, unless in the proximity of a domain wall, one would not expect to observe changes in spin direction. Thus the atoms of a given surface would appear identical, even given the use of a magnetic tip and even in the presence of applied magnetic fields.

A recent work (2004) by Berdunov et al. presents a unique experiment using SP-STM to examine the spin-structure of FM magnetitite ($Fe_3O_4$).[56] Magnetite is currently of great interest for its possible use as a spin-injection electrode in devices such as magnetic tunnel junctions. Berdunov et al. present interesting results on the (111) face of $Fe_3O_4$. Their sample surface was produced using an oxidizing procedure which results in a stable oxygen termination. The surface structure then consists of a lattice of O atoms (first layer) on top of an Fe layer (second layer). With only few surface O vacancies, the surface forms a hexagonal superstructure having periodicity of ~42 Å, which is explained as being due to an electron-lattice instability.[57]

Berdunov et al. study this surface using magnetic STM tips in a UHV STM system at room temperature. For the magnetic tip, they chose to use a MnNi alloy in the form of rods which are electrochemically etched to produce sharp tips. MnNi (1:1 stoichiometry) is an aFM compound with a high Néel temperature (~800 °C) having the tetragonal CuAu-I type structure, one of a family of such materials.[58–61] One advantage of an aFM tip is to avoid possible stray field effects on the sample under study.

To explore the success of the MnNi tip preparation procedure, an Auger spectroscopy study was performed on a similarly prepared MnNi disk.[62] In fact, this study indicated preferential sputtering during the final *in-vacuum* preparation (ion etching) step, leaving a Ni-rich phase.[58] If this also occurs for the case of the tip etching, then a thin FM layer might have formed at the tip apex. But in any case, the tip so produced would presumably be spin-polarized with small, or negligible, stray field.

Under zero applied magnetic field, Berdunov et al. obtained STM images like that reproduced in Figure 8(a), which shows extended areas of bright and dark, corresponding to the large-scale superstructure. The little protrusions are interpreted as the O atom sites, whose spacing depends on the exact location within the superstructure, but is ~3 Å. A number of small O vacancies are observed, which appear as holes [circled in the image of Fig. 8(a)]. No sign of any spin-polarized effect is seen in this image.

Under a magnetic field of 60 mT applied parallel to the surface of the sample, a different image was obtained, as reproduced in Figure 8(b). This image shows the same superstructure features as with no magnetic field. However, it shows that in the vicinity of the O vacancy sites, there appear three bright spots, which are not seen in the absence of applied magnetic field. The height of the bright spots in relation to the surrounding O sites is measured to be ~0.3 Å. The separation of the bright spots (6 Å) and their positions are stated to correspond to the positions of Fe ions in the layer underneath the topmost O layer. According to the authors, the bright spots have a magnetic origin.

Berdunov et al. apply the basic tunneling equation (which assumes a constant sample LDOS) at the position of the bright spot and also at the position of an O site,

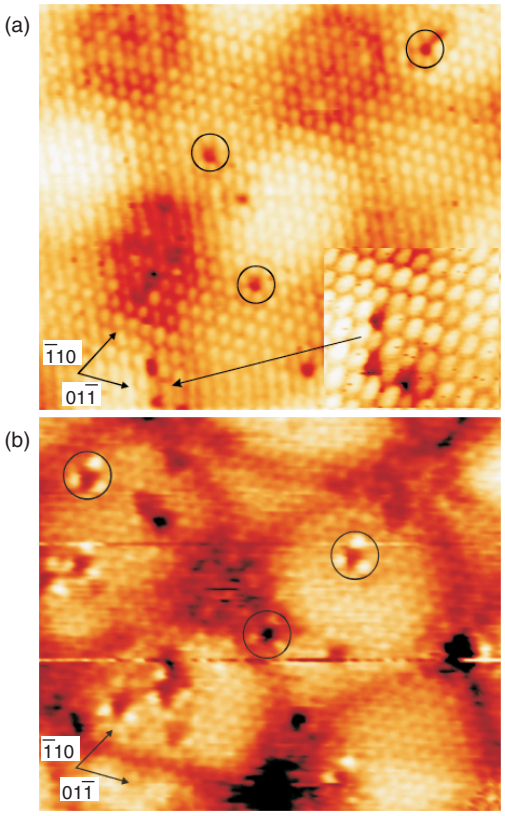


**Fig. 8.** STM images ($10.5 \times 8.5$ nm$^2$ and $7 \times 8$ nm$^2$) of the superstructure without (a) and with magnetic field (b). Circles mark the oxygen vacancies in the topmost surface layer. (b) Three bright spots appear around vacancies that correspond to Fe sites with 6 Å interatomic distance. ($V_{\text{bias}} = -1.0V, I_t = 0.1$ nA, MnNi tip). Inset in (a) shows a high resolution image of the defects. Reprinted with permission from [56], N. Berdunov et al., *Phys. Rev. Lett.* 93, 057 201 **(2004)**. © 2004, American Physical Society.

in order to determine the tunneling conductance at those points. From these numbers, the conductance variation is determined to be ~250%, showing that the bright spots represent a sizeable spin-polarized effect.

To understand more clearly what the origin of the conductance increase at the Fe site under the applied *in-plane* magnetic field is, other experiments and some calculations were also reported. For example, Berdunov et al. reported in another paper that vibrating sample magnetometry measurements indicated that 60 mT is sufficient to fully saturate the magnetization of the sample.[63] In their related paper, Murphy et al. state that they expect that the sample has *out-of-plane* ([111]-oriented) magnetization in zero-field, but that the applied 60 mT field rotates the magnetization to *in-plane*.[58] However, this by itself still does not explain the enhancement above the Fe sites near the O vacancies, since their magnetization is assumed to be parallel to that of the rest of the sample.

To find a plausible explanation of the observed effect, it is necessary to consider the effect of the O vacancy on the LDOS of the sample, in particular on the spin-polarized LDOS. According to a previous paper by Tsymbal et al., the surface O-atom orbitals of the ideal O-terminated surface (without vacancies) become conductive through hybridization of the O *p*-states with the transition metal (Fe) *d*-states.[64] According to the plots of spin-polarized DOS shown by Berdunov et al., obtained from their first-principles calculations, the surface O sites then become spin-polarized just as with the underlying Fe atom sites. This is particularly true over the range from the Fermi level to 1 eV below the Fermi level, which corresponds to the energy window ($V_{\text{bias}} = -1$ V) of their experimental SP-STM image. The spin-polarization over this window is, however, much larger for the second-layer Fe states than for the surface O states.

To understand the obtained magnetic effect as explained by Berdunov et al., it is necessary to consider that in the vicinity of the O vacancy, the spin-polarization of the Fe states is altered, presumably due to changes in the hybridization of *p* and *d* orbitals. Plausibly, this could result in a local increase in the spin-polarization at the Fe atom sites directly adjacent to the O vacancy. In their paper, the authors present plots of spin-up electron density above the O-terminated surface, both with and without an O vacancy. Clearly, the spin-up electron density at specific sites is altered by the presence of the vacancy.

From the experimental point of view, however, this still does not explain why the bright features were not seen in the image under zero applied magnetic field, using spin-polarized STM with the MnNi tip. A plausible explanation (not put forth by Berdunov et al.) could be that by applying the *in-plane* magnetic field, the magnetization of the sample was rotated into alignment with the magnetic vector of the tip. In this case, then, the spin-polarized tunneling current could be enhanced at the point with greatest spin-polarized LDOS, such as above the Fe atoms adjacent to the O vacancy. This would imply that the magnetization of the MnNi tip was parallel to the sample surface. In absence of applied field, magnetization vectors of sample and tip would be orthogonal, resulting in no spin-polarized contrast.

In any case, the results presented by Berdunov and co-workers in their recent series of papers represents a very interesting observation of atomic-resolved spin-polarized imaging. The ability to detect local changes in the spin-polarization of ferromagnets, down to the atomic scale, opens new vistas for the technique of atomic-resolved SP-STM.

## 5. THEORETICAL BASIS FOR ATOMIC SCALE SPIN-RESOLVED STM

In tandem with the various atomic-scale SP-STM experiments which have been reported within the last 5 years, a variety of theoretical studies have also been published. Many of these studies have been performed in collaboration with the experimental efforts, though not all. In this

section is discussed the current state of the art in theories of atomic-scale SP-STM, including comparative discussions across the range of published experimental results.

### 5.1. Fourier Expansion in Reciprocal Lattice Vectors: Star Functions and Star Coefficient Theory

#### *5.1.1. Magnetic Signal Dominant*

The original paper of Heinze et al. on the topic of Mn ML/W(110) was a combination of theory and experiment.[7] Shortly thereafter (2001), Wortmann and colleagues published a second, theory-only paper in which they laid down basic theory of spin-polarized tunneling and then applied it to make SP-STM simulations of a Cr ML on Ag(111).[16] In that paper is introduced the extension of the Tersoff-Hamann equation to the spin-polarized case, and an expression is given for the tunneling current in terms of the nonmagnetic and magnetic LDOS of sample and tip, similar to Eq. (2) given here.

The paper of Wortmann et al. reiterated the point made in Heinze et al.'s work that the magnetic signal in CC imaging mode of Mn ML/W(110) dominated completely the chemical atom (nonmagnetic) signal. And in their STM simulations of Cr/Ag(111), a model spin-frustration system, the same effect is also predicted.

The theory for this behavior is explained well within the work of Heinze et al. and Wortmann et al., namely, in terms of the reciprocal lattice vectors $G_{\|}$ of the magnetic structure in comparison to those of the nonmagnetic structure. As explained, an SP-STM image can be written as a 2D Fourier expansion in reciprocal lattice vectors, in which the $G_{\|}$'s appear in the expansion coefficients as exponents of damped exponentials. Therefore, the larger the $G_{\|}$, the smaller the expansion coefficient. As the nonmagnetic lattice will have the largest $G_{\|}$'s, it will be the most strongly damped.

Bode et al., in a very thorough and explicatory paper (2002), defined the reciprocal lattice vector Fourier expansion in terms of "star functions" and "star coefficients".[65] The star coefficient theory applied to Mn ML/W(110) is also discussed at length in another paper by Heinze et al.[66] This theory strengthened the reciprocal lattice vector theory by considering that the electronic states of the surface, relevant to specific length scales, are contained within the star "coefficients". Hereafter, I refer to this theory as the star coefficient theory.

#### *5.1.2. Magnetic Signal a Perturbation*

The star coefficient theory, with which the recent (2005) work of Kubetzka et al. on Fe/W(001) is in good agreement, preceded the work of Yang et al.'s 2002 paper, in which it was shown that both magnetic and nonmagnetic contrast were obtained in, and could be separated from, a single atomic-scale SP-STM image of aFM $Mn_3N_2$(010).[14]

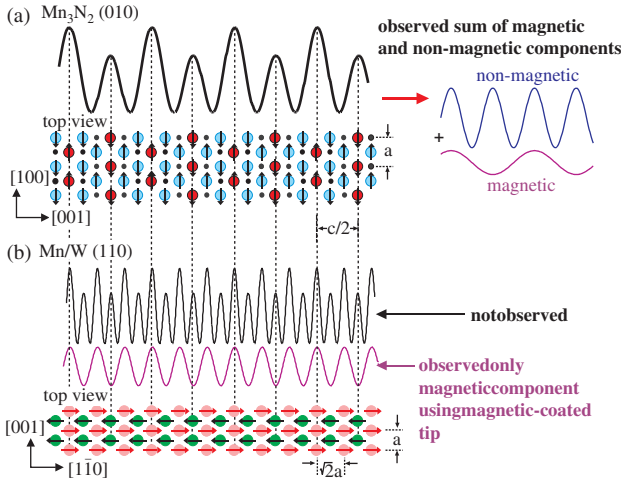


**Fig. 9.** Comparative diagram between SP-STM results on $Mn_3N_2$(010) by Yang et al. and Mn ML/W(110) by Heinze et al. (a) Schematic total line profile with top view surface model of $Mn_3N_2$(010) and separated components; (b) schematic line profile obtained (only magnetic) with top view surface model of Mn ML/W(110). Also shown is the fictitious total line profile including the nonmagnetic part which was not obtained. Surface models have been normalized to have the same $x$-direction atomic row spacing. Reprinted with permission from [37], A. R. Smith et al., *Recent Adv. Atomic-Scale Spin-Polarized Scanning Tunneling Microsc., Microsc. Res. Technique* 66, 72 (**2005**). © 2005, Wiley-Liss, Inc.

In Figure 9 is reproduced from Ref. [37] a comparitive diagram between the SP-STM results on $Mn_3N_2$(010) of Yang et al. and the Mn ML/W(110) of Heinze et al. As can be seen, the spatial arrangement of Mn atoms is very similar for the two different systems. In either case, the surface Mn atoms form a centered rectangular lattice with their magnetic moments alternating in direction from row to row, with rows along [100] for $Mn_3N_2$(010) and along [001] for Mn/W(110). Although the lattice constants and a:b ratios are slightly different, for comparison purposes in Figure 9 the two lattice models have been normalized along the $x$-direction.

It is also important to note the existence of two chemically inequivalent Mn atom sites on $Mn_3N_2$(010), Mn1 and Mn2. As discussed thoroughly in Ref. [37], the result is that the two inequivalent Mn sites completely change the nonmagnetic periodicity of the surface. Since the magnetic superstructure of $Mn_3N_2$ (010) has a period of six individual atomic rows, compared to the case of Mn/W(110) of two individual atomic rows, the associated reciprocal lattice vectors (magnetic and nonmagnetic) are comparatively smaller; therefore, one may expect that it will be possible to observe both the magnetic and nonmagnetic components.

It should be noted, however, that in Yang et al.'s work, the nonmagnetic signal has *larger* amplitude than the magnetic signal at all measured bias voltages between $-1.0$ and $+1.0$ V; this behavior would therefore seem to not necessarily agree with the predictions of the star coefficient theory. However, it may not disagree, if the spin-polarized electronic states of the sample, and the electronic structure of the STM tip as well, are taken into account.

In fact, Bode et al. discuss the importance of first-principles calculations to identify the electronic states contained within the particular star coefficients, noting that if there are no states contained within the star coefficient of the smallest nonvanishing reciprocal lattice vector, then the STM image will be dominated instead by the star function of the next larger reciprocal lattice vector.

The case of $Fe_3O_4(111)$ reported by Berdunov et al. may also be reconsidered in comparison with the star coefficient theory. As reproduced in Figure 8(b), it is clear that in the applied-field case, the magnetic protrusion is a feature which is superimposed on the oxygen corrugation. Berdunov et al. state in their paper that the bright spots seen under applied field correspond with the positions of the underlying Fe atoms having spacing of 6 Å; whereas, the surface O atom spacing is only ~3 Å. We may therefore consider that the star wavefunction corresponding to the Fe atoms has the smallest reciprocal lattice vectors and should therefore be dominant in the image. And in fact, this appears to be the case, compared with the O atom corrugation surrounding the bright spots. From this perspective, the $Fe_3O_4(111)$ case is consistent with star coefficient theory.

Finally, we may reconsider the case of NiO(001) imaged using SP-AFM with magnetic-coated tips, as reported by Hosoi and co-workers. Clearly, as reproduced in Figure 7(d), the magnetic corrugation is truly a tiny modulation on top of the nonmagnetic corrugation, despite the fact that the reciprocal lattice vectors corresponding to the magnetic unit cell are the smallest nonzero ones. We can therefore say with fair certainty that the star coefficient theory does not hold for atomic-scale SP-AFM; but this is not unreasonable, since the exchange force imaging mechanism is completely different and needs more study.

#### *5.1.3. Atomic-Scale Magnetic Imaging Using* $\mathbf{d}I/\mathbf{d}V$ *Mode*

Along with CC mode magnetic imaging at the atomic scale, Wortmann et al.[16] discuss briefly the spectroscopic mode, considering that the derivative of the tunneling current equation has the form

$$\mathrm{d}I_t/\mathrm{d}V \sim \frac{1}{2}[n^t n^s + m^t m^s \cos\theta] \qquad (3)$$

Eq. (3) is the basis for the highly successful application of the spectroscopic $\mathrm{d}I/\mathrm{d}V$ mode utilized by Wiesendanger and co-workers to obtain the dramatic results on domains and domain walls of various transition metal surfaces.[2–10] It is so successful because the $\mathrm{d}I/\mathrm{d}V$ mode allows the magnetic signal to be locked at a specific voltage where it is maximized and it is not overwhelmed by the nonmagnetic (topographic) signal.

Despite this advantage, Wortmann et al. argued that the $\mathrm{d}I/\mathrm{d}V$ method was inapplicable to reveal complex atomic-scale spin structures, partly due to the perceived resolution limitation in $\mathrm{d}I/\mathrm{d}V$ imaging to about 1 nm; this turns out not to be a limit at all, as reproduced in Figure 6(c) from the recent (2005) work of Kubetzka et al., who show $\mathrm{d}I/\mathrm{d}V$ resolution of single atoms (nearest neighbor spin-↑–spin-↑ atom spacing of 4.476 Å). Kubetzka et al. have certainly shown that the $\mathrm{d}I/\mathrm{d}V$ mode is applicable to atomic-scale SP-STM measurements.

### 5.2. Inclusion of Tip Electronic Structure

Without a doubt, the spin-polarized electronic structure of the STM tip plays a crucial role in atomic-scale SP-STM. In this section are described theoretical calculations in which the electronic structure of the tip is included.

#### *5.2.1. Case of Mn ML on W(110)*

In a paper published subsequent to Heinze et al.'s 2000 work on the Mn ML on W(110), Hofer and Fisher revisit the magnetic STM imaging of that surface using first-principles theory, with the intent to determine the extent to which current theory is able to reproduce the parameters observed in the experiment.[67] In their paper, they describe their theoretical work in which they compute the STM currents and corrugations using Bardeen's integral.[68] Several interesting points were determined from their analysis.

First of all, Hofer and Fisher not only computed the ground state of the pseudomorphic Mn/W(110) system, they also compute the electronic properties of the tip, assuming particular models for the tip. The first key result which they find concerns the simulation using the clean W tip. Interestingly, they found a corrugation of only 0.02 Å, as compared with Heinze et al.'s experiment, which found a nonmagnetic corrugation of 0.15 Å. Bode et al. explain this discrepancy as a well-known deficiency of the Tersoff-Hamann model in predicting atomic-resolved corrugations of close-packed metal surfaces and also relate it to the diminishingly small size of the associated third star coefficient in comparison to the second star coefficient.[65]

On the other hand, calculated STM images using an Fe-atom tip (Fe apex atom on a W film) resulted in the opposite effect, namely, a magnetic image having the same qualitative symmetry as found in Heinze et al.'s experiment but a corrugation of 0.73 Å, in comparison to the much smaller corrugation found in the experiment of 0.03–0.04 Å (Fe-coated W tip) or <0.01 Å (Gd-coated W tip). Hofer and Fisher also present their result for a Mn-atom tip (Mn apex atom on a W film), finding a much reduced magnetic corrugation of 0.18 Å. While it may be supposed that a further corrugation reduction could occur due to misalignment of the tip and sample magnetic axes, Hofer and Fisher conclude that in the actual experiment of Heinze et al., the tip had most likely become coated with Mn atoms from the surface.

In a subsequent (2003) paper, Hofer and Fisher show new calculations in which they consider specific tip models of even more direct relevance to the actual experiment, particularly considering Fe atom tips contaminated with various amounts of Mn.[69] They show explicitly, for different tip models, the corresponding theoretical STM images with associated predicted corrugations. An interesting finding is that a dramatic reduction in corrugation amplitude occurs (0.89 Å $\Rightarrow$ 0.04 Å) upon replacing a Mn-contaminated tip (modeled as an Fe(100) facet tipped with a single Mn apex atom) with a highly Mn-contaminated tip (modeled as an Fe(100) facet coated with a Mn layer and tipped with a Mn apex atom).

Lastly, we consider the tunneling current question. In Hofer and Fisher's calculations for Mn ML/W(110), the median tip–sample distance used was 4.5 Å, corresponding to a tunneling current of 0.1 nA (Fe-atom tip) or 0.2 nA (Mn-atom tip). These typical STM tunneling currents are to be compared with the actual value reported (40 nA) for the experiment of Heinze et al. Such a large tunneling current would, in Hofer and Fisher's simulation, put the tip–sample system so close as to be in mechanical instability.[70] Reasoning further, they conclude that no method of STM simulation, based on ground-state density functional theory, can explain the high current quoted in the experiment. A possible explanation for this discrepancy is found in their more recent (2003) paper.[69]

#### *5.2.2. Case of Fe ML/W(001)*

It is interesting to hypothetically extend these results to the case of the aFM Fe ML/W(001) recently reported experimentally by Kubetzka et al.[43] For a Fe tip (modeled as an Fe(100) facet tipped with an Fe apex atom) applied to the Mn ML/W(110), Hofer and Fisher predict a theoretical corrugation of 0.68 Å. Thus it would suggest that Fe-coated W tips should normally be capable of high atomic-scale corrugations. However, in the reported experiment on Fe ML/W(001), in which Fe-coated W tips were used, the measured CC corrugation was slightly less than 0.03 Å, and, since these data were acquired with applied magnetic field (+2.5 T) which forced the tip magnetization vector perpendicular to the surface, combined with the *out-of-plane* anisotropy of the Fe ML deduced in the experiment, the tip and sample magnetizations should have been collinear during the measurement. Based on that, it is reasonable to assume that 0.03 Å represents the maximum corrugation achievable in the experiment. And there could have been no possibility of Mn contamination in this experiment. It would be therefore interesting to know what corrugations would be predicted by theory for the Fe ML/W(001) for various types of tips.

Concerning the tunneling current in the case of Fe ML/W(001), Kubetzka et al. reported a value of just 3 nA for the image reproduced here in Figure 6. However, in the other STM figure of their paper, they report a value of 30 nA. Possibly the same explanation for the large tunneling current in the Mn ML/W(110) case would apply to this case, since both experiments were performed in the same STM system.

#### *5.2.3. Case of $Mn_3N_2$(010)*

The $Mn_3N_2$(010) surface offers exciting possibilities for testing atomic-scale SP-STM both experimentally and theoretically. In a previous section, original data of Smith and co-workers have been displayed, which shows that the magnetic properties of this surface are both interesting and complex. The complexity arises upon considering that the size of the magnetic period is a full six primitive atomic rows. Contained within that magnetic period are two rows of Mn1 atoms and four rows of Mn2 atoms. Therefore, in theoretical calculations, one must take into account the electronic states from both the Mn1 and Mn2 atoms. The corresponding size of the magnetic unit cell renders these calculations highly nontrivial. The N atoms have much lower LDOS and so contribute little to the tunneling current.

Concerning the key parameters of the SP-STM experiment on $Mn_3N_2$(010), it is noted that while the bias voltage ranged from $-1.0$ V to $+1.0$ V, the tunneling current used was quite typical, i.e., 0.3 nA (Fig. 4 data). The magnetic amplitude reached a maximum of $\sim$0.07 Å at $V_S = -0.15$ V, but it decreases to zero at $V_S \simeq +0.4$ V; above 0.4 V, the magnetic corrugation becomes negative due to the polarization reversal. The nonmagnetic amplitude for the same data set reached a maximum of $\sim$0.26 Å at $V_S = +0.1$ V and gets smaller in either direction. Note that the maximum magnetic contrast is larger than the magnetic contrast reported by either Heinze et al. or Kubetzka et al.

Dick and Neugebauer have recently (2004) reported first-principles density functional theory calculations for the $Mn_3N_2$(010) surface.[15] The theory used in this work is based simply on the spin-generalized Tersoff-Hamann model. The local density of states is first calculated using plane waves; however, to overcome certain calculational problems encountered for tip–sample distances $>3$ Å, the wavefunctions were projected from the plane wave basis onto a basis set of atomic orbitals. Various tip models are utilized in order to generate the simulated STM images.

To compare with the experimental data at one interesting bias point, the Tersoff-Hamann simulations were carried out at $V_S = -0.2$ V. In the simulation, the tip–surface distance was 5 Å with effective tip spin polarization of 90%. Using these parameters, and with a single atom tip, the Tersoff-Hamann simulation found a total SP-STM height profile showing very little magnetic modulation; decomposition of the profile into its magnetic and nonmagnetic parts revealed the reason why. The magnetic profile was highly oscillatory, showing magnetic

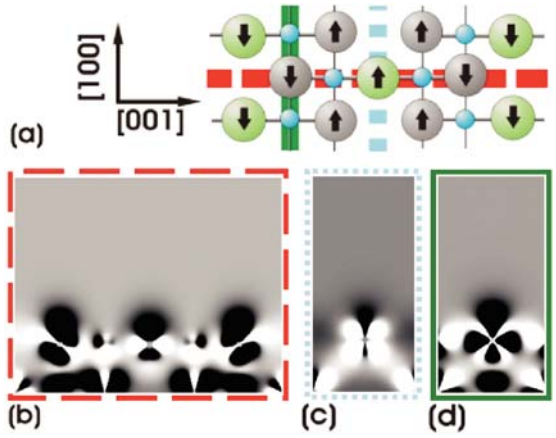


**Fig. 10.** (a) Schematic view of the atomic and magnetic structure of the top surface layer. The arrows inside the atoms indicate the sign of the magnetic moment as determined by ILDOS at bias voltage $V_s = -0.2$ V, i.e., by integrating corresponding LDOS over a sphere around each atom and over energy. (b), (c), and (d) show contour plots of the magnetic LDOS for the case of $V_s = -0.2$ V, where bright and dark regions correspond to spin-up and spin-down densities correspondingly. The contour plots shown are the cross sections through the surface layer along the [001] axis (b) and the [100] axis (c, d). Horizontal and vertical bars of (a) show cross section position of (b), (c), and (d). Reprinted with permission from [15], A. R. Smith et al., Aspects of spin-polarized scanning tunneling microscopy at the atomic scale: experiment, theory, and simulation. *Surf. Sci.* 561, 154 (**2004**). © 2004, Elsevier.

contrast at each of the six Mn atomic rows which are aFM (see Ref. [15]). The nonmagnetic corrugation was 0.36 Å, while the magnetic corrugation was 0.17 Å. Comparing this result with the corresponding atom-superposition simulation illustrated a key point regarding spin-polarized Tersoff-Hamann, that it is not the sphere-integrated (around the surface atom nucleus) LDOS which is most relevant, but instead the highly directional orbital lobes probed by the STM tip.

In the $Mn_3N_2(010)$ case, the relevant surface orbital lobes were mainly of Mn sd character. Contour plots of the magnetic spin density (LDOS) for $Mn_3N_2(010)$, together with a schematic view of the atomic and magnetic structure of the top surface layer, are reproduced from Ref. [15] in Figure 10. What is nicely seen in Figure 10 is that, e.g., for the central Mn atom, its sphere-integrated magnetic LDOS is positive (spin-↑); whereas in the region at the surface probed by the STM tip, the spin density is clearly negative (spin-↓).

#### *5.2.4. $Mn_3N_2(010)$: A Multiatom Tip Apex Model*

Because of this orbital lobe directionality, the single magnetic atom tip in Tersoff-Hamann simulation resulted in an aFM period of only two atomic rows for $Mn_3N_2(010)$ at $V_S = -0.2$ V, not seen in the experiment. However, to reproduce the experiment, Dick and Neugebauer have not applied the star coefficient theory but rather have continued with Tersoff-Hamann directly and instead applied a multiatom tip apex. In particular, they applied a 4-atom magnetic tip consisting of four noninteracting *s*-like atoms located at the corners of a square and lying in a plane parallel to the surface.

Corrugation profiles based on this 4-atom tip apex model are shown in Ref. [15]. Essentially, the 4-atom tip results in overall very good agreement with the experiment. The total corrugation profile appears as a modulated sinusoid as in the experiment, and the separated components have both the correct shape and periodicity of the experimental ones. Numerically, the nonmagnetic component has a corrugation of 0.19 Å, a little smaller than in the experiment (0.24 Å), whereas the magnetic component has a corrugation of 0.05 Å, also a little smaller than in the experiment (0.07 Å). Note, however, that the predicted magnetic corrugation would be approximately a factor of 2 smaller if an effective tip polarization of 44% was used, similar to that assumed for Fe-coated W tips by Bode et al.[3] Dick and Neugebauer also explored the effect of varying the tip apex atom-to-atom distance as well as the tip–surface distance, and those effects are also described in Ref. [15].

#### *5.2.5. Case of $Fe_3O_4(111)$*

Lastly, it is interesting to briefly reconsider the case of $Fe_3O_4$ (111) reported by Berdunov et al.[56] quantitatively. The tunneling conditions certainly are typical for STM ($V_{bias} = -1.0$ V, $I_t = 0.1$ nA). The corrugation difference between the magnetic feature (bright spot) and the surrounding atomic structure was reported to be 0.3 Å. Compared with the measurements already discussed for aFM surfaces, this experimental magnetic corrugation is actually quite large [more than 4× as large as the maximum magnetic corrugation measured for $Mn_3N_2(010)$, 0.07 Å], especially considering that the signal is attributed to the enhanced magnetization of a second-layer Fe atom; of course, a strong hybridization between surface O states and second-layer Fe states was found. It would be interesting, however, to have a calculation which tries to take into account the tip structure.

## 6. SUMMARY

This paper has attempted to provide the reader with a reasonably thorough discussion of recent advances in spin-resolved probe microscopy, mainly tunneling microscopy, including a number of the chief experimental works as well as important theoretical papers. Overall, it is found that major progress has been made in this field within 6 years (c. 2000–2005). Experiments have succeeded to resolve exceedingly fine details of magnetic structure of various surfaces and to determine ground-state magnetic structures in systems where non-SPM-based experimental methods could only obtain evidence indirectly. Truly, the atomic-resolved SP-STM represents the ultimate in 2D spin-resolving techniques.

Tersoff-Hamann theory has been successfully extended to the atomic-scale spin-polarized case and, in combination with first-principles density functional theory, has been applied with great success to model the experimental results. A variation of this, referred to as star coefficient theory, has been discussed and its validity examined. In general, it appears to describe well many of the experimental findings. The electronic structure of the STM tip remains an apparent key ingredient in the STM calculations. Future theoretical work will not likely avoid taking it into account.

In the future, we may expect that experimentalists will continue to surprise with further dramatic displays of spin-resolved surface structures. Going beyond this, the day may not be far off when experimentalists succeed at engineering specific magnetic structures at the atomic scale and, using the power of SP-STM, directly verify their magnetic structure step by step.

**Acknowledgments:** The author acknowledges support from the National Science Foundation (Grant nos. 9983816 and 0304314) and also from the Office of Naval Research (Grant nos. N00014-99-1-0528 and N00014-05-1-0418).

## References and Notes


1. G. Binnig, H. Rohrer, C. Gerber, and E. Weibel, *Appl. Phys. Lett.* 40, 178 (**1982**).
2. R. Wiesendanger, H.-J. Guntherodt, G. Guntherodt, R. J. Gambino, and R. Ruf, *Phys. Rev. Lett.* 65, 247 (**1990**).
3. M. Bode, M. Getzlaff, and R. Wiesendanger, *Phys. Rev. Lett.* 81, 4256 (**1998**).
4. R. Wiesendanger, M. Bode, and M. Getzlaff, *Appl. Phys. Lett.* 75, 124 (**1999**).
5. O. Pietzsch, A. Kubetzka, M. Bode, and R. Wiesendanger, *Science* 292, 2053 (**2001**).
6. M. Bode, S. Heinze, A. Kubetzka, O. Pietzsch, X. Nie, G. Bihlmayer, S. Blügel, and R. Wiesendanger, *Phys. Rev. Lett.* 89, 237 205 (**2002**).
7. S. Heinze, M. Bode, A. Kubetzka, O. Pietzsch, X. Nie, S. Blügel, and R. Wiesendanger, *Science* 288, 1805 (**2000**).
8. M. Kleiber, M. Bode, R. Ravlic, and R. Wiesendanger, *Phys. Rev. Lett.* 85, 4606 (**2000**).
9. A. Kubetzka, M. Bode, O. Pietzsch, and R. Wiesendanger, *Phys. Rev. Lett.* 88, 057 201 (**2002**).
10. A. Kubetzka, O. Pietzsch, M. Bode, and R. Wiesendanger, *Phys. Rev. B* 88, R020401 (**2003**).
11. S. N. Okuno, T. Kishiand, and K. Tanaka, *Phys. Rev. Lett.* 88, 066 803 (**2002**).
12. E. Y. Vedmedenko, A. Kubetzka, K. V. Bergmann, O. Pietzsch, M. Bode, J. Kirschner, H. P. Oepen, and R. Wiesendanger, *Phys. Rev. Lett.* 92, 077 207 (**2004**).
13. T. K. Yamada, M. M. J. Bischoff, G. M. M. Heijnen, T. Mizoguchi, and H. V. Kempen, *Phys. Rev. Lett.* 90, 056 803 (**2003**).
14. H. Q. Yang, A. R. Smith, M. Prikhodko, and W. R. L. Lambrecht, *Phys. Rev. Lett.* 89, 226 101 (**2002**).
15. A. R. Smith, R. Yang, H. Yang, W. R. L. Lambrecht, A. Dick, and J. Neugebauer, *Surf. Sci.* 561, 154 (**2004**).
16. D. Wortmann, S. Heinze, Ph. Kurz, G. Bihlmayer, and S. Blügel, *Phys. Rev. Lett.* 86, 4132 (**2001**).
17. C. L. Fu and A. J. Freeman, *Phys. Rev. B* 33, 1755 (**1986**).
18. S. Blugel, D. Pescia, and P. H. Dederichs, *Phys. Rev. B* 39, 1392 (**1989**).
19. M. Bode, M. Getzlaff, and R. Wiesendanger, *Phys. Rev. Lett.* 81, 4256 (**1998**).
20. R. Wiesendanger, M. Bode, A. Kubetzka, O. Pietzsch, M. Morgenstern, A. Wachowiak, and J. Wiebe, *J. Mag. Mag. Mat.* 272, 2115 (**2004**).
21. M. Bode, M. Hennefarth, D. Haude, M. Getzlaff, and R. Wiesendanger, *Surf. Sci.* 432, 8 (**1999**).
22. G. W. Wiener and J. A. Berger, *J. Met.* 7, 360 (**1955**).
23. F. Lihl, P. Ettmayer, and A. Kutzelnigg, *Z. Metallk.* 53, 715 (**1962**).
24. W. J. Takei, R. R. Heikes, and G. Shirane, *Phys. Rev.* 125, 1893 (**1962**).
25. M. Mekata, *J. Phys. Soc. Jpn.* 17, 796 (**1962**). M. Mekata, J. Haruna, and H. Takei, *J. Phys. Soc. Jpn.* 25, 234 (**1968**).
26. N. Otsuka, Y. Hanawa, and S. Nagakura, *Phys. Stat. Sol.* (*a*) 43, K127 (**1977**).
27. H. Jacobs and C. Stuve, *J. Less Common Metals* 96, 323, (**1984**).
28. G. Kreiner and H. Jacobs, *J. Alloys Compounds* 183, 345 (**1992**).
29. M. Tabuchi, M. Takahashi, and F. Kanamaru, *J. Alloys Compounds* 210, 143 (**1994**).
30. K. Suzuki, T. Kaneko, H. Yoshida, Y. Obi, H. Fujimori, and H. Morita, *J. Alloys Compounds* 306, 66 (**2000**).
31. A. Leineweber, R. Niewa, H. Jacobs, and W. Kockelmann, *J. Mat. Chem.* 10, 2827 (**2000**).
32. T. Dietl, H. Ohno, F. Matsukura, J. Cibert, and D. Ferrand, *Science* 287, 1019 (**2000**).
33. H. Yang, H. Al-Brithen, A. R. Smith, J. A. Borchers, R. L. Cappelletti, and M. D. Vaudin, *Appl. Phys. Lett.* 78, 3860 (**2001**).
34. H. Q. Yang, H. Al-Brithen, A. R. Smith, E. Trifan, and D. C. Ingram, *J. Appl. Phys.* 91, 1053 (**2002**).
35. H. Q. Yang, R. Yang, A. R. Smith, and W. R. L. Lambrecht, *Surf. Sci.* 548, 117 (**2003**).
36. W. R. L. Lambrecht, M. Prikhodko, and M. S. Miao, *Phys. Rev. B* 68, 174 411 (**2003**).
37. A. R. Smith, R. Yang, H. Q. Yang, A. Dick, J. Neugebauer, and W. R. L. Lambrecht, *Microscopy Res. and Tech.* 66, 72 (**2005**).
38. J. Tersoff and D. R. Hamann, *Phys. Rev. Lett.* 50, 1998 (**1983**). J. Tersoff and D. R. Hamann, *Phys. Rev. B* 31, 805 (**1985**).
39. R. Yang, H. Q. Yang, A. R. Smith, A. Dick, and J. Neugebauer, *Phys. Rev. B* (**2006**), accepted.
40. G. A. Mulhollan, R. L. Fink, J. L. Erskine, and G. K. Walters, *Phys. Rev. B* 43, 13 645 (**1991**).
41. J. Chen and J. L. Erskine, *Phys. Rev. Lett.* 68, 1212 (**1992**).
42. R. Wu and A. J. Freeman, *Phys. Rev. B* 45, R7532 (**1992**).
43. A. Kubetzka, P. Ferriani, M. Bode, S. Heinze, G. Bihlmayer, K. von Bergmann, O. Pietzsch, S. Blügel, and R. Wiesendanger, *Phys. Rev. Lett.* 94, 087 204 (**2005**).
44. K. von Bergmann, M. Bode, A. Kubetzka, O. Pietzsch, and R. Wiesendanger, *Micr. Res. Tech.* 66, 61 (**2005**).
45. K. Mukasa, H. Hasegawa, Y. Tazuke, K. Sueoka, M. Sasaki, and K. Hayakawa, *Jpn. J. Appl. Phys.* 33, 2692 (**1994**).
46. H. Ness and F. Gautier, *Phys. Rev. B* 52, 7352 (**1995**).
47. K. Nakamura, H. Hasegawa, T. Oguchi, K. Sueoka, K. Hayakawa, and K. Mukasa, *Phys. Rev. B* 56, 3218 (**1997**). K. Nakamura, T. Oguchi, H. Hasegawa, K. Sueoka, K. Hayakawa, and K. Mukasa, *Appl. Surf. Sci.* 140, 366 (**1999**).
48. A. S. Foster and A. L. Shluger, *Surf. Sci.* 490, 211 (**2001**).
49. H. Hosoi, K. Sueoka, and K. Mukasa, *Nanotechnology* 15, 505 (**2004**).
50. K. Sueoka, A. Subagyo, H. Hosoi, and K. Mukasa, *Nanotechnology* 15, S691 (**2004**).
51. M. Bammerlin, R. Lüthi, E. Meyer, A. Baratoff, J. Lü, M. Guggisberg, C. Gerber, L. Howard, and H.-J. Güntherodt, *Probe Microsc.* 1, 3 (**1997**).
52. S. Ciraci, A. Baratoff, and I. P. Batra, *Phys. Rev. B* 41, 2763 (**1990**).

**53.** M. R. Castell, S. L. Dudarev, G. A. D. Briggs, and A. P. Sutton, *Phys. Rev. B* 59, 7342 **(1999)**.
**54.** L. N. Kantrovich, A. L. Shluger, and A. M. Stoneham, *Phys. Rev. B* 63, 184 111 **(2001)**.
**55.** H. Momida and T. Oguchi, *Surf. Sci.* 590, 42 **(2005)**.
**56.** N. Berdunov, S. Murphy, G. Mariotto, and I. V. Shvets, *Phys. Rev. Lett.* 93, 057 201 **(2004)**.
**57.** I. V. Shvets, N. Berdunov, G. Mariotto, and S. Murphy, *Europhys. Lett.* 63, 867 **(2003)**.
**58.** S. Murphy, S. F. Ceballos, G. Mariotto, N. Berdunov, K. Jordan, I. V. Shvets, and Y. M. Mukovskii, *Microsc. Res. Technol.* 66, 85 **(2005)**.
**59.** J. S. Kasper and J. S. Kouvel, *J. Phys. Chem. Sol.* 11, 231 **(1959)**.
**60.** W. B. Pearson, K. Brun, and A. Kjekshus, *Acta Chem. Scand.* 19, 477 **(1965)**.
**61.** L. Pál, E. Krén, G. Kádár, P. Szabó, and T. Tarnóczi, *J. Appl. Phys.* 39, 538 **(1968)**.
**62.** S. F. Ceballos, G. Mariotto, S. Murphy, and I. V. Shvets, *Surf. Sci.* 523, 131 **(2003)**.
**63.** N. Berdunov, S. Murphy, G. Mariotto, I. V. Shvets, and Y. M. Mykovskiy, *J. Appl. Phys.* 95, 6891 **(2004)**.
**64.** E. Y. Tsymbal, O. N. Mryasov, and P. R. LeClaire, *J. Phys. Condens. Matter* 15, R109 **(2003)**.
**65.** M. Bode, S. Heinze, A. Kubetzka, O. Pietzsch, M. Hennefarth, M. Getzlaff, R. Wiesendanger, X. Nie, G. Bihlmayer, and S. Blügel, *Phys. Rev. B* 66, 014 425 **(2002)**.
**66.** S. Heinze, P. Kurz, D. Wortmann, G. Bihlmayer, and S. Blügel, *Appl. Phys. A* 75, 25 **(2002)**.
**67.** W. A. Hofer and A. J. Fisher, *Surf. Sci.* 498, L65 **(2002)**.
**68.** J. Bardeen, *Phys. Rev. Lett.* 6, 57 **(1961)**.
**69.** W. A. Hofer and A. J. Fisher, *J. Mag. Mag. Mat.* 267, 139 **(2003)**.
**70.** W. A. Hofer, A. J. Fisher, R. A. Wolkow, and P. Grütter, *Phys. Rev. Lett.* 87, 236 104 **(2001)**.

Received: 9 January 2006. Accepted: 28 February 2006.